AIChE

Bimodal Micro-Mesoporous Aluminosilicates for Heavy Oil Cracking: Porosity Tuning and Catalytic Properties

Qingfeng Tan
State Key Laboratory of Heavy Oil Processing, China University of Petroleum, Changping, Beijing 102249, P.R. China

Yu Fan, Haiyan Liu, Tengchun Song, Gang Shi, and Baojian Shen
The Key Laboratory of Catalysis, China National Petroleum Corporation, China University of Petroleum, Changping, Beijing 102249, P.R. China

Xiaojun Bao
State Key Laboratory of Heavy Oil Processing, China University of Petroleum, Changping, Beijing 102249, P.R. China

The Key Laboratory of Catalysis, China National Petroleum Corporation, China University of Petroleum, Changping, Beijing 102249, P.R. China

DOI 10.1002/aic.11512
Published online May 7, 2008 in Wiley InterScience (www.interscience.wiley.com).

Through a two-step synthesis procedure, bimodal micro-mesoporous aluminosilicates, denoted as B-MASs, were synthesized by assembling preformed zeolite Y nanoclusters using a triblock polymer as template. By controlling the aging conditions of preformed zeolite nanoclusters the porosity of the B-MASs was suitably tuned. The characterization results showed that the pore walls of the mesoporous phase in the B-MASs consist of zeolite Y nanoclusters and the microporosity of the B-MASs is inherited from the incorporated nanoclusters. It was suggested that more incorporation of the well-developed zeolite nanoclusters accounts for the increasing microporosity of the B-MASs with the increasing aging temperature of the preformed zeolite nanoclusters. The incorporated nanoclusters have much shorter pore channels and mainly contribute weak Lewis acid sites to the B-MASs. The resulting bimodal micro-mesoporous materials B-MASs with mutually connected mesopores and shorter micropores showed superior catalytic properties when used for cracking heavy crude oil. © 2008 American Institute of Chemical Engineers *AIChE J,* 54: 1850–1859, 2008
Keywords: bimodal micro-mesoporous aluminosilicates, zeolite nanoclusters; pore structure tuning, heavy oil catalytic cracking

Introduction

Since their emergence, mesoporous materials such as MCM-41 and SBA-15 have attracted considerable attention because of their potential applications in separation and catalysis involving large molecules.[1–3] Compared with conventional microporous zeolites, however, these mesoporous materials have much weaker acidity and lower hydrothermal stability because of the amorphous nature of their mesoporous walls.[4] Although the incorporation of heteroatoms such as aluminum can generate catalytically active sites, the hydrothermal stability of the resulting aluminum-substituted

Correspondence concerning this article should be addressed to X. J. Bao at baoxj@cup.edu.cn.

mesostructural materials often become lower.[5,6] These shortages severely limit their industrial applications, especially those dealing with high-temperature operations with steam such as encountered in petroleum fluid catalytic cracking (FCC). Therefore, to improve the hydrothermal stability and increase the acidity of mesoporous materials has been the focus of mesoporous material research.[7]

On the other hand, microporous zeolites have been the most widely used porous inorganic materials in catalysis because of their adjustable acidity and well-defined micropores. Although the micropores of various zeolites usually less than 1 nm confer the exceptional properties in various size-selective reactions,[8] their intrinsic smaller pore size brings diffusional limitations, especially when used for converting bulky molecules. It has been recognized that hierarchical pore structure that combines the advantages of both mesoporous materials and microporous zeolites can offer attractive features and circumvent the problems aforementioned.[9,10] There have been several successful examples regarding the synthesis of such hierarchical porous materials, such as by compositing mesoporous materials with zeolites[11,12] and by creating mesoporosity in zeolite crystals.[13,14] Nevertheless, the diffusion path length in the micropore channels of these composite materials is still quite long for diffusion-limited reactions,[15] because of the bulky and separate nature of microporous zeolites in these composite materials.[16] Such a quite long diffusion path length often results in much longer time for intermediate product molecules inside micropore channels to diffuse outward, leading to unwanted by-reactions such as excessive cracking in FCC processes. So, to fully take advantage of the unique adsorption performance and excellent shape-selectivity of microporous zeolites without suffering from diffusional limitations, micropore channels in zeolite phase should be short[17] and directly connected to more open mesopores, as described by the concept of pore continuum.[18] This suggests the necessity to create so-called bimodal pore system that can substantially enhance the accessibility of the catalytically active sites existing in microporous channels and thereby increase the catalytic efficiency, because molecules to be converted are first transported through the mesopore channels and then adsorbed in the micropores to undergo selective catalytic reactions. An effective approach to preparing such bimodal porous materials is to endow ordered mesoporous materials with some characteristics of microporous zeolites, i.e., to generate zeolitic microporosity and acidity within the pore walls of ordered mesoporous materials.[19] For this purpose, steam-stable aluminosilicates MSUs,[20] named after their invention institution Michigan State University, and hydrothermally stable mesoporous aluminosilicates (MASs)[21,22] have been successfully synthesized via the assemblage of zeolite nanoclusters/seeds using surfactant-templated synthesis in both alkaline and acidic media. By recrystallizing the pore walls, mesoporous materials with semicrystalline zeolitic framework were also obtained.[23] Although numerous results have shown that the ratio of microporosity to mesoporosity in such bimodal porous materials has remarkable influence on the catalytic efficiency of the resulting catalysts in terms of conversion, yield, and product selectivity,[9,24] the porosity control of bimodal porous materials is still a great challenge.

In this article, a series of bimodal micro-mesoporous aluminosilicates (B-MASs) with tunable microporosity were prepared by assembling zeolite Y nanoclusters in an acidic medium. The resulting materials were characterized by X-ray diffraction (XRD), Fourier transformed infrared spectroscopy (FTIR), transmission electron microscopy (TEM), N_2 adsorption, ^{27}Al solid-state nuclear magnetic resonance (^{27}Al NMR) spectroscopy, in-situ FTIR spectroscopy of adsorbed pyridine (Py-IR), and differential thermogravimetry (DTG). The catalytic activities of the samples were assessed in a microactivity testing (MAT) unit using heavy oil catalytic cracking as a model reaction system.

Experimental

Materials

Sodium silicate (containing 26.0 wt % SiO_2) was purchased from Beijing Hongxing Chemicals (China). Aluminum sulfate (containing 99.0 wt % $Al_2(SO_4)_3 \cdot 18H_2O$) and sodium hydroxide (containing 96.0 wt % NaOH) were purchased from Beijing Yili Fine Chemicals (China). $EO_{20}PO_{70}EO_{20}$ (Pluronic P123) was purchased from Aldrich (USA).

Synthesis procedure

A typical synthesis procedure of the B-MASs with different microporosities is described as follows: (1) Five mixtures with the identical molar ratio of Na_2O:Al_2O_3:SiO_2:H_2O at 16:1.0:15:300 were prepared in parallel by mixing 4.6 g sodium silicate, 0.9 g aluminum sulfate, and 1.25 g sodium hydroxide in 4.8 mL deionized water in five autoclaves under stirring, and then aged under stirring at 45, 70, 95, 120, 140°C for 24 h, respectively, to obtain five solutions of zeolite Y nanoclusters; (2) Five P123 solutions were prepared in parallel by dissolving 2.08 g P123 in 52.6 mL H_2O and mixing with 10.0 mL H_2SO_4 of 2.5 M/L, to each of them one of the preformed zeolite Y nanocluster solutions obtained in step (1) was added, and the pH values of the resulting gels were adjusted to 2.0 by dropwise adding a H_2SO_4 solution of 2.5 M/L; (3) The resulting five gel mixtures were stirred at 40°C for 20 h and then transferred into five autoclaves to crystallize at 100°C for 24 h, the crystallization products were collected by filtration, then dried in air, and calcined at 550°C for 6 h to remove the template to obtain five B-MAS samples denoted as B-MAS-1, B-MAS-2, B-MAS-3, B-MAS-4, and B-MAS-5, respectively.

For comparison purpose, an aluminum-substituted SBA-15, which was named after its invention institution University of California, Santa Barbara, was prepared by the direct synthesis method described in literature[25] under the same conditions used for synthesizing the B-MASs, except for that the nanocluster solution was replaced by an equivalent amount of sodium silicate and aluminate. Zeolite Y was prepared by statically crystallizing the third nanocluster solution (aged at 95°C) at 100°C for 24 h.

Characterizations

The XRD patterns of the samples were obtained on a Shimadzu 6000 diffractometer (Shimadzu, Japan) using CuKα radiation and operated at 40 kV and 30 mA. TEM characterization was conducted on a JEOL-2000FX II electron micro-

Table 1. Properties of the Heavy Crude Oil Feedstock

Items	Vacuum gas oil	Vacuum residual oil
Density (20°C) (g/cm^3)	0.8748	0.9310
100°C viscosity (mm^2/s)	11.28	137.67
Conradson carbon (m%)	0.30	8.22
Initial boiling point (°C)	423	456
500°C distilled (m%)	38	7
Element analysis (m%)		
C	85.94	86.62
H	13.70	12.67
N	0.20	0.30
S	0.16	0.41

scope (JEOL, Japan) operated at 120 kV. The FTIR spectra of the samples were recorded on a Nicolet Magna-IR 560 E. S. P. spectrometer (Nicolet, USA) with a resolution of 1 cm^{-1}. N_2 adsorption and desorption isotherms were measured on an ASAP 2020M instrument (Micromeritics, USA) at liquid nitrogen temperature. The Brunauer-Emmett-Teller (BET) method was used to calculate the surface areas of the samples (S_{BET}). The surface areas (S_{Mic}) and volumes (V_{Mic}) of micropores were calculated by using the V-t plot method.[26] The sizes of mesopores were derived from Barrett-Joyner-Halenda (BJH) models. The values of unit cell parameter were calculated using the formula $a = 2d_{100}/3^{1/2}$, where d_{100} represents the d-spacing value of the (100) diffraction peak in the XRD patterns. The values of wall thickness d were calculated by subtracting mesopore size (b) from unit cell dimension (a). ^{27}Al solid-state NMR experiments were performed on a Varian Unity Inova 300 spectrometer (Varian, USA) equipped with a double resonance 6 mm Chemagnetics^{TM} MAS probe and operated with frequency at 59.59 MHz, pulse width at 1.5 μs, radiofrequency field strength at 50 G, pulse delay at 2 s, spinning rate at 5 kHz, and 10,000 scans. Pyridine adsorption experiments were conducted on self-supported wafers in an in-situ FTIR cell. The samples were dehydrated at 500°C for 5 h under a vacuum of 1.33×10^{-3} Pa and the adsorption of purified pyridine vapor at room temperature for 20 min was followed. The system was then evacuated at different temperatures (200 and 350°C) and the FTIR spectra were recorded. The DTG analysis was performed on a STA409PC thermogravimetric analyzer (Netzsch, Germany) at a heating rate of 5°C/min in air.

Catalytic cracking performance tests

The H-form samples of the above B-MASs, Al-SBA-15, and zeolite Y were obtained by repeated procedure of ion exchange with a NH_4NO_3 solution of 1.0 M/L and calcination at 550°C for 2 h. The H-form samples were then pressed into pellets, crushed, sieved to 20–40 mesh, and finally steamed before being used as catalysts.

Heavy crude oil catalytic cracking tests were carried out in a MAT unit by the pulse method. The heavy crude oil feedstock used was a blend of 30 wt % Daqing (China) vacuum residue and 70.0 wt % Daqing vacuum gas oil. The physical and chemical properties of the feedstock are shown in Table 1. The heavy crude oil catalytic cracking tests were performed under the standard conditions: catalyst loading 4.0 g; reaction temperature 500°C; 1.3 g of the heavy crude oil was introduced to the reactor through an injection tube within 60 s, then purging nitrogen was followed for 5 min. Before entering the reactor, the feedstock was preheated to 90°C to improve its flowability. The reaction products were collected in a gas collector and a liquid collector, respectively, through a cooling bath. The component analyses of the cracking products were carried out using an Agilent gas chromatographer equipped with a flame ionization detector.

Results and Discussion

Characterization

XRD. Figure 1 shows the XRD patterns of the calcined B-MAS-1, B-MAS-2, B-MAS-3, B-MAS-4, B-MAS-5, and Al-SBA-15 samples before and after the hydrothermal treatment in 100% water vapor at 800°C for 2 h, and Table 2 lists the corresponding structural parameters. Each of the B-

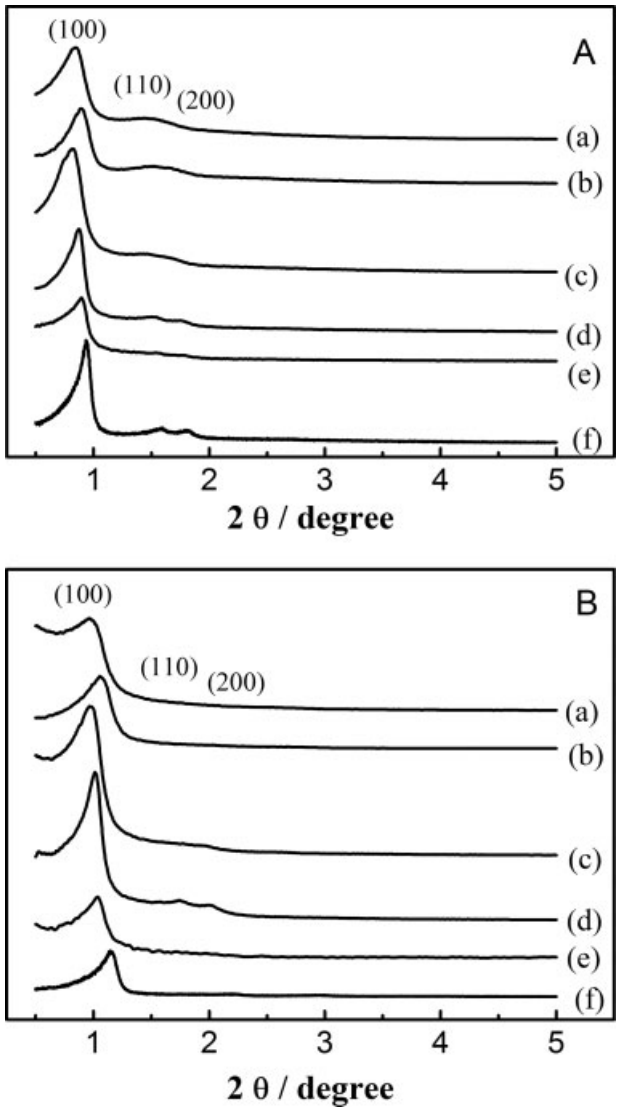

Figure 1. XRD patterns of (a) B-MAS-1, (b) B-MAS-2, (c) B-MAS-3, (d) B-MAS-4, (e) B-MAS-5, and (f) Al-SBA-15 before (A) and after (B) the treatment in 100% water vapor at 800°C for 2 h.

Table 2. d_{100} Values (d_{100}), Unit Cell Parameters (a), Mesopore Diameters (b), Pore Wall Thicknesses (d), BET Surface Areas (S_{BET}), Total Pore Volumes (V_T), Micropore Surface Areas (S_{Mic}), Micropore Volumes (V_{Mic}), Mesopore Volumes (V_{Mes}), Distance Between Two Neighboring Mesopores Estimated from TEM (a_{TEM}), Mesopore Size Estimated from TEM (b_{TEM}), and Mesopore Wall Thickness Estimated from TEM (d_{TEM}) of the Calcined B-MAS and Al-SBA-15 Samples

Samples	Aging temperature of nanoclusters (°C)	D_{100} (nm)	a (nm)	b (nm)	d (nm)	S_{BET} (m^2/g)		V_T (cm^3/g)		S_{Mic} (m^2/g)	V_{Mic} (cm^3/g)	V_{Mes} (cm^3/g)	V_{Mic}/V_{Mes}	a_{TEM} (nm)	b_{TEM} (nm)	d_{TEM} (nm)
						Before HT*	After HT	Before HT	After HT							
B-MAS-1	45	10.38	11.99	7.46	4.53	700.6	121.5	1.001	0.321	66.8	0.037	0.964	0.04	12.00	7.50	4.50
B-MAS-2	70	9.91	11.45	6.91	4.55	646.0	129.8	0.833	0.288	111.0	0.061	0.772	0.08	11.50	6.90	4.60
B-MAS-3	95	10.69	12.34	6.28	6.06	653.5	144.7	0.766	0.330	171.1	0.093	0.673	0.14	12.40	6.30	6.10
B-MAS-4	120	10.05	11.61	6.43	5.18	716.3	168.6	0.732	0.345	238.8	0.129	0.603	0.21	11.60	6.40	5.20
B-MAS-5	140	9.85	11.38	6.49	4.89	702.9	162.0	0.728	0.339	262.7	0.141	0.587	0.24	11.40	6.50	4.90
Al-SBA-15		8.90	10.30	6.30	4.00	695.0	92.3	0.810	0.210	82.6	0.022	0.788	0.04	10.40	6.20	4.20

*HT denotes the hydrothermal treatment in 100% water vapor at 800°C for 2 h.

MAS samples has well-resolved diffraction peaks associated with the ordered hexagonal arrays of mesopores of uniform size (Figures 1A, curves a–e). The absence of the diffraction peaks in the high angle region (5–35°) of the XRD patterns of the five B-MAS samples (not shown) suggests that they are pure mesoporous phase without bulky zeolite crystals. It is interesting to note that the d_{100} values reflecting the (100) interplanar spacings of the five B-MAS samples are larger than that of the Al-SBA-15 sample (Table 2). Combining the results of the N_2 adsorption–desorption experiments shown in Table 2, we can see that the wall thickness of the five B-MAS samples is also thicker than that of the Al-SBA-15 sample. This phenomenon is attributed to the relatively larger spatial volume and stronger rigidity of the preformed zeolite nanoclusters used for synthesizing the B-MASs than the non-structured silicon and aluminium species used for synthesizing Al-SBA-15.[27] Furthermore, the (110) and (200) peaks of the five B-MAS samples (Figure 1A, curves a–e) are relatively less visible and distinguishable than those of the Al-SBA-15 sample (Figure 1A, curve f), suggesting that the mesopores in the five B-MAS samples are relatively not as ordered as those in the Al-SBA-15 sample. This is because the relatively larger spatial volume and stronger rigidity of zeolite nanoclusters make the assembly relatively difficult and thus result in relatively less order of the mesophase in the final products.[22] Interestingly, after the hydrothermal treatment in 100% water vapor at 800°C for 2 h, the five B-MAS samples (Figure 1B, curves a–e) show stronger (100) diffraction peak intensity than the Al-SBA-15 sample (Figure 1B, curve f), although before the hydrothermal treatment the latter (Figure 1A, curve f) shows stronger (100) diffraction peak intensity than the formers (Figure 1A, curves a–e), indicating the higher hydrothermal stability of the formers than the latter.

It is well known that the chemical and physical properties of mesoporous materials are strongly dependent on their preparation conditions.[1,2] In the case of the B-MASs, the key synthesis factor is the preformation of zeolite Y nanoclusters. These zeolite Y nanoclusters undergo the surfactant-templated assembly and form the mesoporous products B-MASs. The XRD patterns of the solid products obtained by filtrating the five nanocluster solutions reveal some representative features of nano-faujasite (Figure 2, curves a–e), while the zeolite Y sample show all the diffraction peaks typical to faujasite crystals in its XRD pattern (Figure 2, curve f). These results suggest that the silicon and alumina species in the five initial solutions have been transformed into primary and secondary structural units of pure zeolite Y crystals, viz., zeolite Y nanoclusters. During the second step, however, part of these nanoclusters is unavoidably dissolved into the acidic medium and their size is diminished to too small to be resolved by the XRD technique. Consequently, the final products B-MASs do not show any diffraction features typical to the corresponding microporous zeolite crystals in the high angle (5–35°) region of their XRD pattern (not shown). Interestingly, by gradually increasing the aging temperature of the nanocluster solutions from 45 to 140°C, the stronger intensity of the diffraction peaks and thereby the more pronounced characteristics of faujasite were observed for the corresponding solid products obtained by filtering the nanocluster solutions (Figure 2, curves a–e), suggesting that the

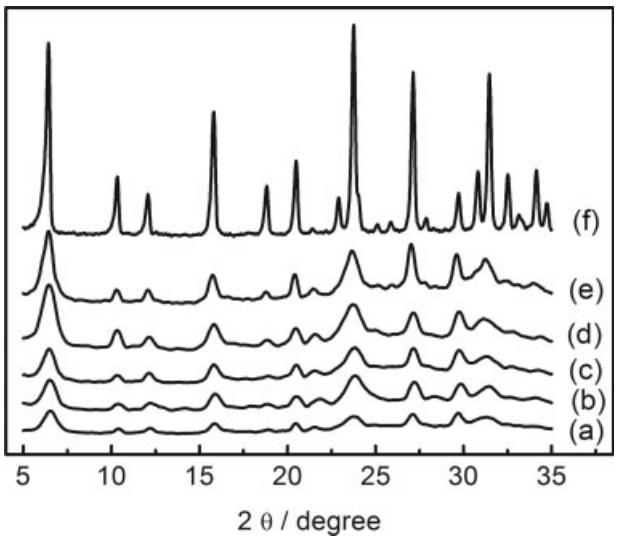

Figure 2. XRD patterns of the solid products obtained by the direct filtration of the nanocluster solutions used for synthesizing (a) B-MAS-1, (b) B-MAS-2, (c) B-MAS-3, (d) B-MAS-4, (e) B-MAS-5, and (f) zeolite Y.

more zeolite nanoclusters with higher matureness were formed in the solutions with the increasing aging temperature.[28]

FTIR. Figure 3 shows the FTIR spectra of the calcined B-MAS-1, B-MAS-2, B-MAS-3, B-MAS-4, B-MAS-5, and Al-SBA-15 samples. Obviously, they all have a broad band at 460 cm^{-1} in the wavenumber region of 400–600 cm^{-1}, similar to that of amorphous materials.[29] For the five B-MAS samples (Figure 3, curves a–e), however, an additional band in the region of 570–580 cm^{-1} is clearly observed. This band is typically ascribed to the double six-member rings of

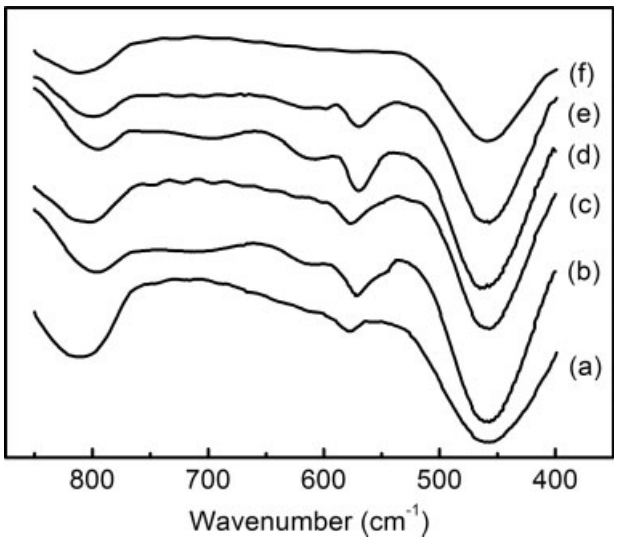

Figure 3. FTIR spectra of the (a) B-MAS-1, (b) B-MAS-2, (c) B-MAS-3, (d) B-MAS-4, (e) B-MAS-5, and (f) Al-SBA-15.

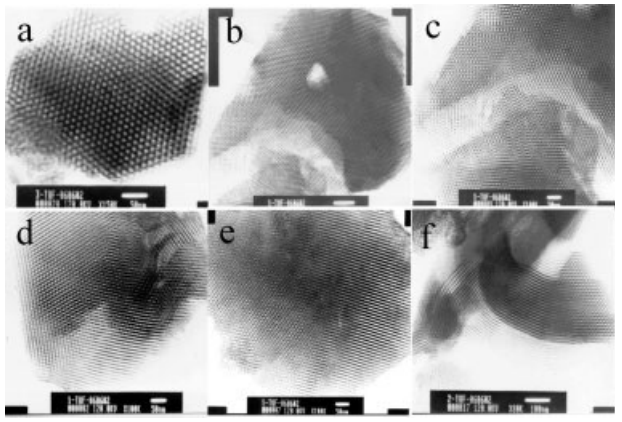

Figure 4. TEM images of the calcined (a) B-MAS-1, (b) B-MAS-2, (c) B-MAS-3, (d) B-MAS-4, (e) B-MAS-5, and (f) Al-SBA-15.

Y type zeolite.[30,31] This result confirms that the nanoclusters containing the structural building units of zeolite Y have been incorporated into the mesoporous walls of the five B-MAS samples, exactly consistent with literature results.[29] This result also indicates that the B-MASs obtained in the present investigation may play the same role as zeolite Y does in catalysis applications.

TEM. The TEM images of the calcined B-MAS-1, B-MAS-2, B-MAS-3, B-MAS-4, B-MAS-5, and Al-SBA-15 samples are shown in Figure 4. Similar to the Al-SBA-15 sample, the five B-MAS samples clearly show the ordered hexagonal arrays of uniform mesopores. From the high black–white contrastness of the TEM images, the distance between two neighboring mesopores and the mesopore wall thickness and size of the five B-MAS samples were estimated and the results are shown in Table 2. The results obtained are basically consistent with those of the XRD analyses.

N_2 Adsorption–Desorption Isotherms. Figure 5 gives the nitrogen adsorption–desorption isotherms of the calcined B-MAS-1, B-MAS-2, B-MAS-3, B-MAS-4, B-MAS-5, and Al-SBA-15 samples before (A) and after (B) the treatment in 100% water vapor at 800°C for 2 h. The isotherms of the five B-MAS samples before the hydrothermal treatment (Figure 5A, curves a–e) show the representative characteristics of type IV adsorption–desorption with a sharp inflection at relative pressure $0.70 < P/P_0 < 0.85$ and a well defined hysteresis loop, similar to that of the Al-SBA-15 sample (Figure 5A, curve f), indicating the well formed mesoporous structure in their frameworks. Interestingly, the isotherms of the five B-MAS samples have a steep increase in N_2 adsorption volume at relative pressure $P/P_0 < 0.01$ (Figure 5A, curves a–e), different from that of the Al-SBA-15 sample (Figure 5A, curve f), suggesting the presence of microporous structure in the five B-MAS samples due to the incorporation of zeolite Y nanoclusters into their pore walls.[21] The approximately linear adsorption volume increments at relative pressure $0.05 < P/P_0 < 0.70$ for the five B-MAS samples are possibly due to the monolayer coverage of regular mesopores by N_2 adsorbate, while the sharp inflections at relative pres-

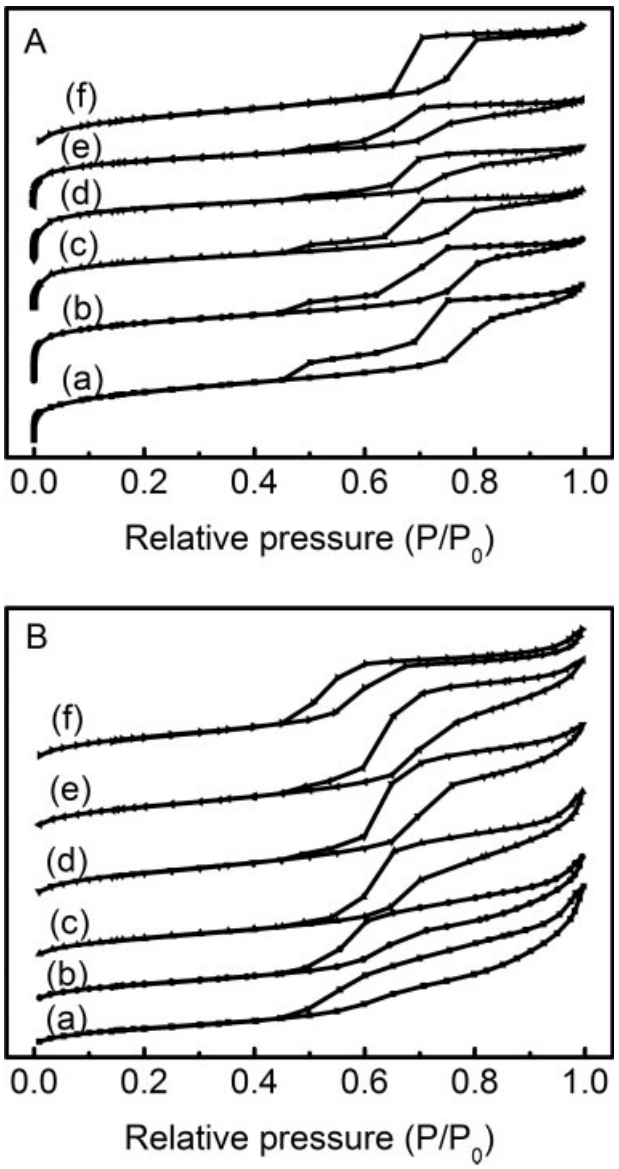

Figure 5. Nitrogen adsorption–desorption isotherms of the (a) B-MAS-1, (b) B-MAS-2, (c) B-MAS-3, (d) B-MAS-4, (e) B-MAS-5, and (f) Al-SBA-15 before (A) and after (B) the treatment in 100% water vapor at 800°C for 2 h.

sure $0.70 < P/P_0 < 0.85$ for the five B-MAS samples indicates the capillary condensation of N_2 adsorbate in their primary mesopores. It is well known that this inflection point on adsorption–desorption isotherms is generally related to the diameter of mesopores and the sharpness of this step indicates the size uniformity of mesopores.[32] The relatively less sharpness of this inflection step and the relatively larger hysteresis loop for the five B-MAS samples (Figure 5A, curves a–e) than those of the Al-SBA-15 sample (Figure 5A, curve f) indicate that the mesopore size of the five B-MAS samples is less uniform than that of the Al-SBA-15 sample, consistent with the above XRD analysis results. Together with the abovementioned XRD and FTIR analysis results, the nitrogen adsorption results introduced here strongly suggest that the five B-MAS samples have a bimodal micro-mesoporous structure. Correspondingly, the five B-MAS samples have surface areas and pore volumes of micropores (Table 2), in addition to their narrowly distributed mesopores (Figure 6). Because no bulky zeolite phase is found in the five B-MAS samples as reflected by the above XRD analysis, it is reasonable to conclude that the microporous structure exists in the mesoporous walls of the B-MASs and thus the micropore channels in the B-MASs should be much shorter than those in ordinary zeolite crystals,[19] because the wall thickness (4.5–6.1 nm, as shown in Table 2) of the mesopores is much smaller than the size (600–800 nm) of ordinary zeolite Y crystals. So, the pore channels of the mesopores and the shorter micropores in the B-MASs are considered to completely run through with each other. Such a pore system consisting of interconnected mesopores and short micropores can greatly improve the accessibility of catalytically active sites in the microporous channels to reactants,[17] especially for reactions taking place in mass transfer limited regime, such as encountered in FCC units operated with heavier feedstock. Also, the micropores of the B-MASs with their size smaller than 1 nm will benefit shape-selective catalysis.

Significantly, Table 2 shows that the change in the preparation conditions of the preformed zeolite nanoclusters leads to a systematic change of the textural properties of the resulting B-MAS samples. For example, by increasing the aging temperature of the preformed zeolite nanoclusters from 45 to 140°C, the remarkable increases in micropore surface area from 66.8 to 262.7 m^2/g and micropore volume from 0.037 to 0.141 cm^3/g are observed for the five B-MAS samples. Generation of microporosity in ordinary SBA-15 materials has been suggested to be from the partial occlusion of hydrophilic poly ethylene oxide (PEO) chains into silica walls.[33,34] The synthesis parameters,[35] including silica/template ratio,[19] crystallization time and temperature level,[19] pH value of mixture,[36] presence of inorganic salt,[37] and length of the

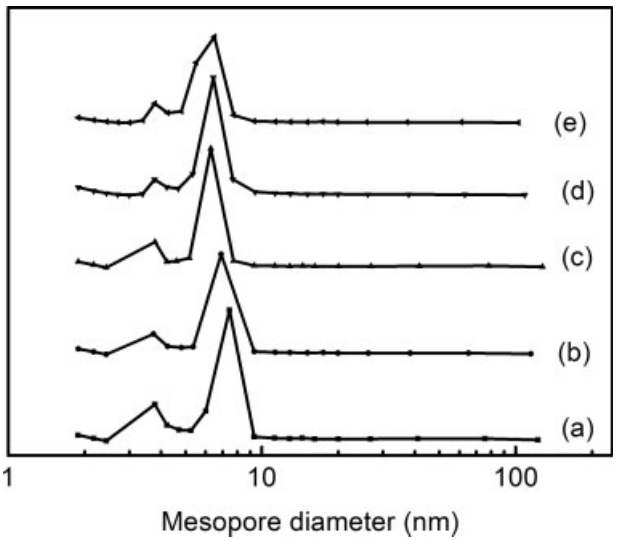

Figure 6. BJH mesopore distributions of the (a) B-MAS-1, (b) B-MAS-2, (c) B-MAS-3, (d) B-MAS-4, (e) B-MAS-5.

EO_n bolck,[38] etc., would affect the microporosity of the resulting SBA-15 due to their influence on the hydrophilicity of PEO chains. However, the present results are quite different from those in literatures: the microporosity in the B-MASs increases only with the increasing aging temperature of the preformed zeolite nanoclusters when the other synthesis parameters such as crystallization temperature and surfactant amount are kept constant. This indicates that the systematic change of microporosity in the B-MASs has nothing to do with the change of hydrophilicity of PEO chains. Simply, the established relationship between the microporosity and the aging temperature of the nanoclusters rules out the effect of the hydrophilicity of PEO chains on the microporosity of the B-MASs.[33,34] So, it is reasonable to deduce that the microporosity in the B-MASs is inherited from the incorporated zeolite nanoclusters in view of their unique synthesis route, and that the increase of microporosity is therefore ascribed to the more incorporation of zeolite nanoclusters with higher matureness as discussed earlier.[22] Although the microporosity and the mesoporosity (mesopore volumes V_{Mes}) of the B-MASs increases and decreases with the increasing aging temperature of the preformed zeolite nanoclusters, respectively, the V_{Mic}/V_{Mes} ratio and the density of microporosity in the mesopore walls of the B-MASs (the density is obtained by dividing the micropore volume by the total pore volume) increase simultaneously (Table 2), and correspondingly, the total porosity (total pore volume V_T) of the B-MASs dereases.

Surprisingly, for the B-MAS samples with higher microporosity, i.e., those prepared from zeolite nanoclusters obtained at higher aging temperatures, higher total surface areas and total pore volumes were retained after the hydrothermal treatment in 100% water vapor at 800°C for 2 h (Table 2), indicating the increased hydrothermal stability. This result was further verified by comparing the N_2 adsorption–desorption isotherms before (Figure 5A, curves a–e) and after (Figure 5B, curves a–e) the hydrothermal treatment. As shown in Figure 5B (curves a–e), the higher the microporosity, the more pronounced characteristics of the typical hexagonal mesostructure the N_2 sorption isotherm of the corresponding B-MAS sample after the hydrothermal treatment has. Prior to the hydrothermal treatment, however, this tendency is reversed (Figure 5A, curves a–e). This result demonstrates that the B-MAS sample with higher microporosity has the higher hydrothermal stability.

^{27}Al NMR. The state of Al in the five B-MAS samples was studied by ^{27}Al solid-state NMR and the results are shown in Figure 7. The only chemical shift for all the five B-MAS samples at 58 ppm (Figure 7, curves a–e) can be assigned to tetrahedrally coordinated Al species, indicating that Al atoms have been incorporated into the framework of the five B-MAS samples. In strongly acidic synthesis media, some metals exist only in cationic form rather than in their oxo species, so free aluminum cations (Al^{3+}) cannot enter the framework of SBA-15 in the conventional synthesis.[39] In our case, Al atoms are directly introduced into the mesostructure in the acidic medium. This can be explained by the fact that Al species are firstly contained in the preformed nanoclusters and subsequently are incorporated into the framework of the products through the templated assembly. Notably, tetrahedral aluminum in the five B-MAS samples

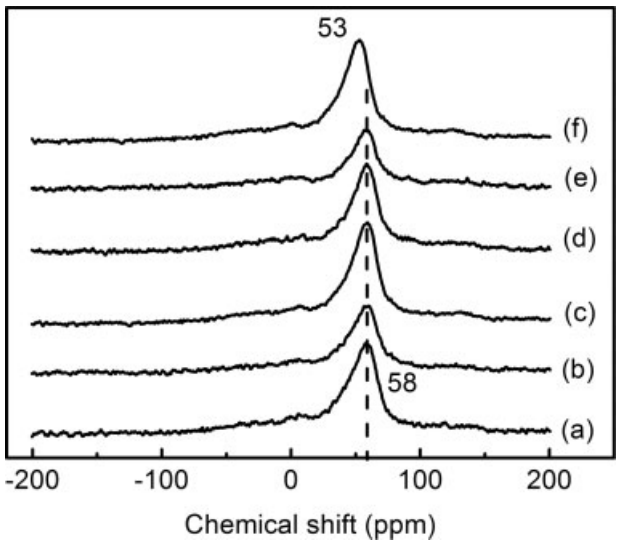

Figure 7. ^{27}Al NMR spectra of the calcined (a) B-MAS-1, (b) B-MAS-2, (c) B-MAS-3, (d) B-MAS-4, (e) B-MAS-5, and (f) Al-SBA-15.

shows ^{27}Al chemical shift at 58 ppm (Figure 7, curves a–e), behaving almost like that in zeolite Y (at ca. 59–61 ppm), but unlike that in Al-SBA-15 (at 53 ppm, Figure 7, curve f). These results reveal that the environment of aluminum in the B-MASs is nearly identical to that in zeolite Y crystals, but significantly different from that in amorphous Al-SBA-15. Given the widely accepted fact that the acidity of zeolitic materials are generally related to the local environment of Al in them,[40] we can expect that the B-MASs obtained in the present investigation should have the similar acidic properties as zeolite Y has.

Py-IR. To understand the influence of microporosity on the acidic properties of the B-MASs, pyridine adsorption experiments of the five B-MAS samples were carried out in in-situ FTIR cells and the results are shown in Figure 8. The two bands at about 1540 and 1450 cm^{-1} are related to the adsorption of pyridine molecules on Brönsted and Lewis acid sites, respectively, and the band at 1490 cm^{-1} is ascribed to the synergistic effects between Brönsted and Lewis acid sites. The quantitative information of Brönsted and Lewis acid sites calculated from pyridine adsorption at 200 and 350°C is listed in Table 3. According to the data, it is clear that with the increasing microporosity from B-MAS-1 to B-MAS-5, the total amount of Brönsted and Lewis acid sites of the corresponding B-MAS sample increases from 527.5 to 1262.4 μmol/g (Table 3). This can be interpreted by the more incorporation of zeolite nanoclusters with higher matureness, as the above XRD and N_2 adsorption analyses have suggested. The increased incorporation of zeolite nanoclustes endows the corresponding B-MAS samples with increased acidity from B-MAS-1 to B-MAS-5. Moreover, from B-MAS-1 to B-MAS-5, the ratio (B/L) of the number of Brönsted acid sites to that of Lewis acid sites decreases from 0.30 to 0.18 and the ratio (W/S) of the number of weak acid sites to that of strong acid sites increases from 1.28 to 2.73. These results indicate that the incorporated zeolite

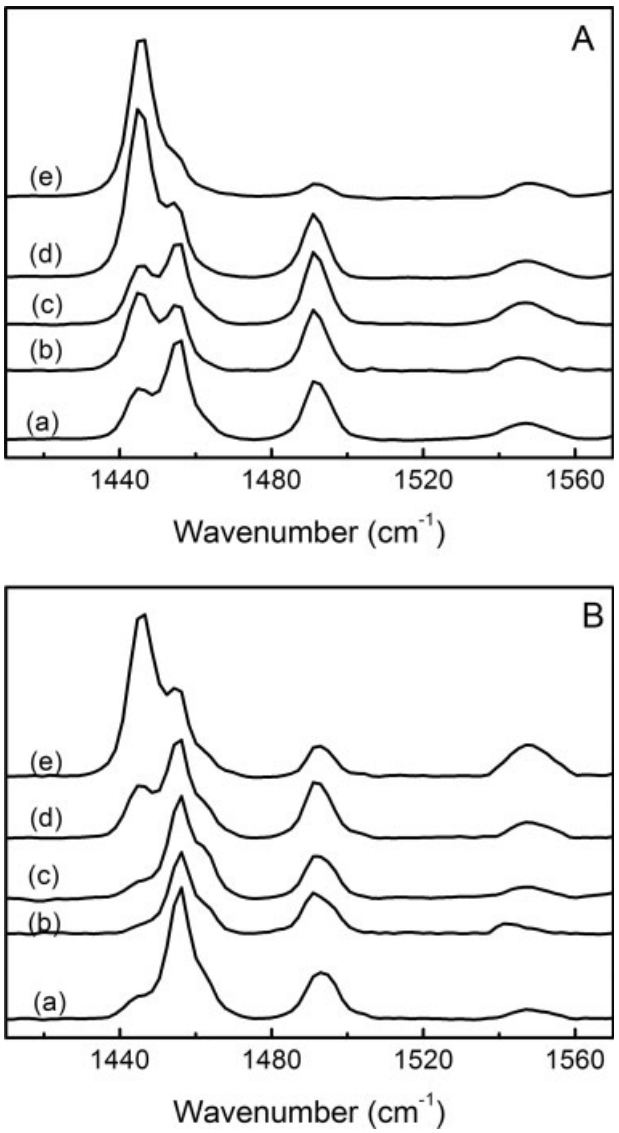

Figure 8. IR spectra of pyridine adsorbed on the protonated (a) B-MAS-1, (b) B-MAS-2, (c) B-MAS-3, (d) B-MAS-4, and (e) B-MAS-5 at (A) 200°C and (B) 350°C, respectively.

nanoclusters contribute more Lewis acid sites than Brönsted acid sites and more weak acid sites than strong acid sites.

DTG Results. The DTG analysis results of the five B-MAS and Al-SBA-15 samples are shown in Figure 9. Obviously, the peak at 284°C on the DTG curve of the Al-SBA-15 sample (curve f) is assigned to the desorption and decomposition of the copolymer template. However, the DTG curves of the B-MAS samples are quite different from that of the Al-SBA-15 sample. The decomposition peaks of the template for the B-MAS samples appear at lower temperature region (180–206°C), which is ascribed to the weaker interaction between the template and the mesopore walls that contain zeolitic nanoclusters.[41] Along with this line, the easier and easier thermal desorption and decomposition of the copolymer template in the samples from B-MAS-1 to B-MAS-5 can be interpreted by the more incorporation of zeolitic nanoclusters with higher matureness, because the incorporated nanoclusters can weaken the adhesion of the template on the walls.[41] This result is also in good agreement with the above N_2 adsorption and pyridine adsorption results.

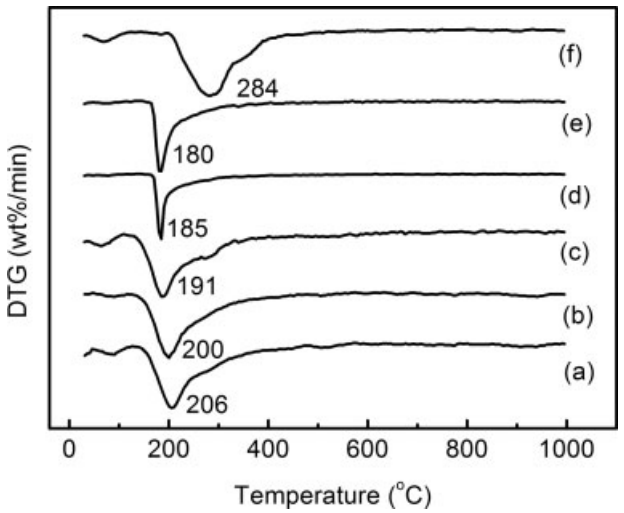

Figure 9. DTG curves of the B-MAS-1 (a), B-MAS-2 (b), B-MAS-3 (c), B-MAS-4 (d), B-MAS-5 (e), and Al-SBA-15 (f) samples.

Catalytic Cracking Results. To explore the catalytic potentials of the B-MASs, three B-MAS samples, i.e., B-MAS-1, B-MAS-4, and B-MAS-5, were selected and tested using heavy oil catalytic cracking as a model reaction system. The results are shown in Table 4, in which the data of the Al-SBA-15 and zeolite Y are also included for comparison purpose. It can be seen that the yields of the light fraction (gasoline + diesel) of the catalysts derived from the three B-MASs are 37.2, 49.3, and 53.4 wt %, respectively, much higher than that (26.7 wt %) of the Al-SBA-15 derived

Table 3. Acidic Properties of the B-MAS Samples

	Py-IR acidity (μmol/g)						
	Brönsted		Lewis				
Samples	Weak	Strong	Weak	Strong	Total	B/L	W/S
B-MAS-1	83.1	37.3	213.1	194.0	527.5	0.30	1.28
B-MAS-2	76.3	39.0	256.0	208.3	579.6	0.25	1.34
B-MAS-3	79.7	32.2	336.9	267.9	716.7	0.19	1.39
B-MAS-4	103.4	62.7	682.1	263.1	1111.3	0.18	2.41
B-MAS-5	116.9	72.9	807.1	265.5	1262.4	0.18	2.73

Table 4. Heavy Crude Oil Catalytic Cracking Results

Samples	Dry gas (wt %)	Liquefied gas (wt %)	Light oil fraction* (wt %)	Heavy cycle oil (wt %)	Coke (wt %)
B-MAS-1	1.2	22.2	37.2	28.6	10.8
B-MAS-4	1.6	18.5	49.3	18.1	12.5
B-MAS-5	1.9	16.3	53.4	14.7	13.7
Al-SBA-15	1.0	12.1	26.7	53.3	6.9
Zeolite Y	2.4	23.1	40.3	16.4	17.8

*Light oil fractions includes gasoline and diesel.

catalyst. This is because the incorporated zeolite nanoclusters in the B-MASs have zeolitic acidity and micoporosity,[41] while having the almost identical surface areas and mesopore sizes as the Al-SBA-15 has (Table 2). For this reason, the three B-MAS sample derived catalysts have their heavy cycle oil (HCO) yields at 28.6, 18.1, and 14.7 wt %, respectively, much lower than that (53.3 wt %) of the Al-SBA-15 derived catalyst. This is consistent with the fact that the B-MASs possess much more acid sites than Al-SBA-15 (365.3 μmol/g, obtained by the Py-IR technique), which also accounts for the higher dry gas and coke yields of the three B-MAS derived catalysts than those of the Al-SBA-15 derived catalyst. Moreover, the dry gas and coke yields of the three B-MAS sample derived catalysts are much lower than those of the zeolite Y derived catalyst (Table 4). This is ascribed, at least partly, to the mesopores in the B-MASs that can promote the outward diffusion of the product molecules and thus greatly reduce the secondary cracking and condensation polymerization reactions, in addition to their relatively lower acidity than zeolite Y (1745.6 μmol/g, obtained by the Py-IR technique). As dry gas and coke come mainly from the secondary cracking and condensation polymerization reactions of product molecules, the much shorter micropore channels in the B-MASs also account for the less yields of dry gas and coke, because the time for the product molecules to diffuse outward through the micropore channels is significantly shortened, i.e., the chance for the product molecules to undergo unwanted secondary cracking and condensation polymerization reaction is greatly depressed. Such an interpretation is perfectly in line with the concept of pore continuum: since the diffusion coefficient of involved molecules in mesopores is several orders of magnitudes larger than that in micropores,[15] the bimodal pore system consisting of interconnected shorter micropores and ordered mesopores in the B-MASs would cause much more rapid transfer of the product molecules than the single micropore structure of bulky zeolite Y crystals.[42] Surprisingly, the B-MAS-4 and B-MAS-5 derived catalysts have their yields of light oil fraction at 49.3 and 53.4 wt %, much higher than that (40.3 wt %) of the zeolite Y derived catalyst, despite that the latter has much more acid sites than the former two. Because the accessibility of catalytically active sites often plays a critical role in diffusion-limited reactions,[9] the enhanced accessibility induced by the mesopores of bimodal pore system in the B-MASs can compensate the relatively lower acidity of their derived catalysts and thus improve the catalytic performance.[42]

For the catalysts derived from the B-MAS samples with the increasing microporosity from B-MAS-1 to B-MAS-5, the decrease in HCO yeild (from 28.6 to 14.7 wt %) and the increase in light fraction (from 37.2 to 53.4 wt %) were observed, mainly due to the increased acidity as the Py-IR analyses have shown. However, the increased microporosity and thereby the increased acidity also result in the increased yields of dry gas and coke from the B-MAS-1 derived catalyst to the B-MAS-5 derived one (Table 4).

In summary, the advantageous pore structure and moderate acidity of the B-MASs make difference. The moderate acidity and zeolitic microporosity of the B-MASs that stand between those of the Al-SBA-15 and zeolite Y result in the higher light oil fraction yields of their derived catalysts than that of the Al-SBA-15 derived catalyst, and the bimodal pore structure of the B-MASs increases the conversion of the heavy feedstock by enhancing the accessibility of catalytically active sites residing in micropores and improve the product selectivity by lessening the unwanted by-reactions.

Conclusions

Bimodal micro-mesoporous aluminosilicates (B-MASs) with high hydrothermal stability and moderate acidity were successfully synthesized by assembling preformed zeolite Y nanoclusters with a triblock polymer as template in an acidic medium. The characterization results showed that the B-MASs contain the nanoclusters of zeolite Y. Significantly, we found that the microporosity of the B-MASs can be suitably tuned by controlling the aging conditions of zeolite nanoclusters, and the B-MAS samples with higher microporosity showed increased hydrothermal stability. It was suggested that the microporosity in the B-MASs is inherited from the incorporated zeolite nanoclusters and the increase of microporosity is due to the more incorporation of zeolitic nanoclusters with higher matureness. The incorporated zeolitic nanoclusters showed the characteristics similar to those of bulky zeolite Y and contributed moderate acidity. When used for cracking heavy crude oil, the B-MAS derived catalysts showed much better catalytic performance than the Al-SBA-15 and zeolite Y derived catalysts because of the advantageous pore structure and moderate acidity. This work demonstrated that the porosity of the bimodal porous materials obtained by nano-assembly can be suitably tuned, which sheds a light for fabricating hierarchical porous materials that have wide applications in separation and catalysis.

Acknowledgments

This work was supported by the National Basic Research Program of China (Grant No. 2004CB217807), the Natural Science Foundation of China (Grant No. 20606037 and 20706059).

Literature Cited

1. Kresge CT, Leonowicz ME, Roth WJ. Ordered mesoporous molecular sieves synthesized by a liquid-crystal template mechanism. *Nature*. 1992;359:710–712.
2. Zhao D, Feng J, Huo Q, Melosh N, Fredrickson GH, Chmelka BF, Stucky GD. Triblock copolymer syntheses of mesoporous silica with periodic 50 to 300 angstrom pores. *Science*. 1998;279:548–552.
3. Jing Z, Maeda H, Ioku K, Ishida EH. Hydrothermal synthesis of mesoporous materials from diatomaceous earth. *AIChE J*. 2007; 53:2114–2122.
4. Corma A. From microporous to mesoporous molecular sieve materials and their use in catalysis. *Chem Rev*. 1997;97:2373–2420.
5. Ooi YS, Zakaria R, Mohamed AR, Bhatia S. Hydrothermal stability and catalytic activity of mesoporous aluminum-containing SBA-15. *Catal Commun*. 2004;5:441–445.
6. Chen LY, Ping Z, Chuah GK, Jaenicke S, Simon G. A comparison of post-synthesis alumination and sol–gel synthesis of MCM-41 with high framework aluminum content. *Microporous Mesoporous Mater*. 1999;27:231–242.
7. Igarashi N, Koyano KA, Tanaka Y, Nakata S, Hashimoto K, Tatsumi T. Investigation of the factors influencing the structural stability of mesoporous silica molecular sieves. *Microporous Mesoporous Mater*. 2003;59:43–52.
8. Ying JY. Nanostructural tailoring: opportunities for molecular engineering in catalysis. *AIChE J*. 2000;46:1902–1906.
9. Ooi Y, Zakaria R, Mohamed AR, Bhatia S. Catalytic conversion of fatty acids mixture to liquid fuel and chemicals over composite microporous/mesoporous catalysts. *Energy Fuels*. 2005;19:736–743.

10. Cooper CA, Lin YS. Synthesis and characterization of silicalite powders and membranes with micro-meso bimodal pores. *J Mater Sci*. 2007;42:320–327.
11. Kloetstra KR, Zandbergen HW, Jansen JC, van Bekkum H. Overgrowth of mesoporous MCM-41 on faujasite. *Microporous Mater*. 1996;6:287–293.
12. Karlsson A, Stocher M, Schmidt R. Composites of micro- and mesoporous materials: simultaneous syntheses of MFI/MCM-41 like phases by a mixed template approach. *Microporous Mesoporous Mater*. 1999;27:181–192.
13. Groen JC, Peffer LAA, Moulijn JA, Perez-Ramirez J. On the introduction of intracrystalline mesoporosity in zeolites upon desilication in alkaline medium. *Microporous Mesoporous Mater*. 2004;69:29–34.
14. Jacobsen CJH, Madsen C, Houzvicka J, Schmidt I, Carlsson A. Mesoporous zeolite single crystals. *J Am Chem Soc*. 2000;122:7116–7117.
15. van Donk S, Janssen AH, Bitter JH, de Jong KP. Generation, characterization, and impact of mesopores in zeolite catalysts. *Catal Rev*. 2003;45:297–319.
16. Petkov N, Holzl M, Metzger TH, Mintova S, Bein T. Ordered micro/mesoporous composite prepared as thin films. *J Phys Chem B*. 2005;109:4485–4491.
17. Prokesova P, Mintova S, Cejka J, Bein T. Preparation of nanosized micro/mesoporous composites via simultaneous synthesis of Beta/MCM-48 phases. *Microporous Mesoporous Mater*. 2003;64:165–174.
18. Le Van Mao R, Al-Yassir N, Nguyen DTT. Experimental evidence for the pore continuum in hybrid catalysts used in the selective deep catalytic cracking of n-hexane and petroleum naphthas. *Microporous Mesoporous Mater*. 2005;85:176–182.
19. Miyazawa K, Inagaki S. Control of the microporosity within the pore walls of ordered mesoporous silica SBA-15. *Chem Commun*. 2000;21:2121–2122.
20. Liu Y, Zhang W, Pinnavaia TJ. Steam-stable MSU-S aluminosilicate mesostructures assembled from zeolite ZSM-5 and zeolite beta seeds. *Angew Chem Int Ed*. 2001;40:1255–1258.
21. Zhang Z, Han Y, Xiao F, Qiu S, Zhu L, Wang R, Yu Y, Zhang Z, Zou S, Wang Y, Sun H, Zhao D, Wei Y. Mesoporous aluminosilicates with ordered hexagonal structure, strong acidity, and extraordinary hydrothermal stability at high temperatures. *J Am Chem Soc*. 2001;123:5014–5021.
22. Han Y, Wu S, Sun Y, Li D, Xiao F, Liu J, Zhang X. Hydrothermally stable ordered hexagonal mesoporous aluminosilicates assembled from a triblock copolymer and preformed aluminosilicate precursors in strongly acidic media. *Chem Mater*. 2002;14:1144–1148.
23. Trong On D, Kaliaguine S. Large-pore mesoporous materials with semicrystallization zeolitic framework. *Angew Chem Int Ed*. 2001;40:3248–3251.
24. Li W, Lu A, Palkovits R, Schmidt W, Spliethoff B, Schuth F. Hierarchically structured monolithic silicalite-1 consisting of crystallized nanoparticles and its performance in the beckmann rearrangement of cyclohexanone oxime. *J Am Chem Soc*. 2005;127:12595–12600.
25. Luan Z, Hartmann M, Zhao D, Zhou W, Kevan L. Alumination and ion exchange of mesoporous SBA-15 molecular sieves. *Chem Mater*. 1999;11:1621–1627.
26. Zhang F, Yan Y, Yang H, Meng Y, Yo C, Tu B, Zhao D. Understanding effect of wall structure on the hydrothermal stability of mesostructured silica SBA-15. *J Phys Chem B*. 2005;109:8723–8732.
27. Han Y, Xiao F, Wu S, Sun Y, Meng X, Li D, Lin S, Deng F, Ai X. A novel method for incorporation of heteroatoms into the framework of ordered mesoporous silica materials synthesized in strong acidic media. *J Phys Chem B*. 2001;105:7963–7966.
28. Xu R, Pang W, Tu K. *Structure and Synthesis Of Zeolite And Molecular Sieves*. Changchun: Jilin University Press, 1987.
29. Wang R, Xu L, Zhao L, Chu B, Hu L, Shi C, Zhu G, Qiu S. Synthesis, characterization, and catalytic activities of mesostructured aluminophosphate assembled with preformed MFI zeolite nanoclusters. *Microporous Mesoporous Mater*. 2005;83:136–144.
30. Xu R, Pang W, Yu J, Huo Q, Chen J. *Chemistry-Zeolites and Porous Materials*. Beijing: Science Press, 2004.
31. Chen CY, Burkrtt SL, Davis ME. Studies on mesoporous materials. I. Synthesis and characterization of MCM-41. *Microporous Mater*. 1993;2:1–17.
32. Huang W, Liu B, Sun F, Zhang Z, Bao X. Synthesis and characterization of thermally stable MCM-41/-Al_2O_3 composite materials. *Microporous Mesoporous Mater*. 2006;94:254–260.
33. Kruk M, Jaroniec M, Ko CH, Ryoo R. Characterization of the porous structure of SBA-15. *Chem Mater*. 2000;12:1961–1968.
34. Imperor-Clerc M, Davidson P, Davidson A. Existence of a microporous corona around the mesopores of silica-based SBA-15 materials templated by triblock copolymers. *J Am Chem Soc*. 2000;122:11925–11933.
35. Vradman L, Titelman L, Herskowitz M. Size effect on SBA-15 microporosity. *Microporous Mesoporous Mater*. 2006;93:313–317.
36. Joo SH, Ryoo R, Kruk M, Jaroniec M. Evidence for general nature of pore interconnectivity in 2-dimensional hexagonal mesoporous silicas prepared using block copolymer templates. *J Phys Chem B*. 2002;106:4640–4646.
37. Newalkar BL, Choudary NV, Turaga UT, Vijayalakshmi RP, Kumar P, Komarneni S, Bhat TSG. Potential adsorbent for light hydrocarbon separation: Role of SBA-15 framework porosity. *Chem Mater*. 2003;15:1474–1479.
38. Kruk M, Jaroniec M, Joo SH, Ryoo R. Characterization of regular and plugged SBA-15 silicas by using adsorption and inverse carbon replication and explanation of the plug formation mechanism. *J Phys Chem B*. 2003;107:2205–2213.
39. Li Y, Zhang W, Zhang L, Yang Q, Wei Z, Feng Z, Li C. Direct synthesis of Al-SBA-15 mesoporous materials via hydrolysis-controlled approach. *J Phys Chem B*. 2004;108:9739–9744.
40. Mazaj M, Logar NZ, Mali G, Tusar NN, Arcon I, Restic A, Recnli A, Kaucic V. Synthesis and structural properties of titanium containing microporous/mesoporous silicate composite (Ti, Al)-Beta/MCM-48. *Microporous Mesoporous Mater*. 2007;99:3–13.
41. Wang S, Dou T, Li Y, Zhang Y, Li X, Yan Z. Synthesisi, characterization, and catalytic properties of stable mesoporous molecular sieve MCM-41 prepared from zeolite mordenite. *J Solid State Chem*. 2004;177:4800–4805.
42. Tan Q, Bao X, Song T, Fan Y, Shi G, Shen B, Liu C, Gao X. Synthesis, characterization, and catalytic properties of hydrothermally stable macro-meso-micro-porous composite materials synthesized via in situ assembly of preformed zeolite Y nanoclusters on kaolin. *J Catal*. 2007;251:69–79.

Manuscript received Oct. 15, 2007, and revision received Mar. 31, 2008.